ABSTRACT

of the Ph.D. Thesis entitled

Synthesis, Spectral Characterization and Structural Analysis of Metal Complexes Containing Acyl Pyrazolone Ligands and Some Inner Transition Metals

To be Submitted to

The Maharaja Sayajirao University of Baroda

For the degree of

DOCTOR OF PHILOSOPHY
in
Chemistry

Submitted By
Mr. Maitrey Travadi

Guidance under
Dr. R. N. Jadeja

Department of Chemistry

Faculty of Science

The Maharaja Sayajirao University of Baroda

April 2024

Abstract of the Thesis

submitted to

THE MAHARAJA SAYAJIRAO UNIVERSITY OF BARODA

for the award of the degree of

DOCTOR OF PHILOSOPHY

in

CHEMISTRY

Research Student	:	Travadi Maitrey Chirantan
Title of Thesis	:	Synthesis, Spectral Characterization and Structural Analysis of Metal Complexes Containing Acyl Pyrazolone Ligands and Some Inner Transition Metals
Supervisor:	:	**Dr. R. N. Jadeja** Associate Professor
Department	:	CHEMISTRY
Faculty	:	SCIENCE
Registration No	:	FOS/2280
Date of Registration	:	30th April 2021

Maitrey Travadi

Dr. R. N. Jadeja

Research Supervisor

Chapter 1: Introduction to coordination chemistry of Inner transition metal complexes, acylpyrazolone ligands and brief literature review.

Progress in Inner Transition Metal Coordination Chemistry

The elements in the periodic table from Ce to Lu and Th to Lr are known as the inner transition metals or f-block elements. Inner transition metal coordination chemistry has seen significant advancement since the 20th century. The unique electronic configurations and properties of lanthanides and actinides have driven this progress. Ligand design, advanced spectroscopic techniques, and computational methods have all played essential roles in furthering our understanding of inner transition metal complexes.

Characteristics of Inner transition metals

Inner transition metal ions, specifically the lanthanides and actinides, possess distinctive characteristics. The chemical reactivity of these ions varies depending on the specific element and oxidation state [1]. The ionic character of inner transition metal ions is influenced by factors such as their oxidation state, electron localization, and their ability to form stable complexes with ligands [1–2]. Their versatile nature allows them to display both ionic and covalent characteristics in different chemical applications. These elements can exhibit a broad spectrum of colours in their compounds, and this coloration is often particularly pronounced in coordination complexes [3]. They have distinctive absorption and emission properties due to their partially filled f-orbitals. Covalency is the property of inner transition metal complexes which refers to the extent of electron sharing between the central metal atom and the surrounding ligands [4]. It is influenced by factors such as the nature of ligands, the oxidation state of the metal ion, orbital overlap, crystal field effects, bonding geometry, and steric hindrance [4,5]. Research on complexes of inner transition elements covers a wide range of applications [6–9].

Acylpyrazolone: Special class of β-diketone ligands

Acylpyrazolones are an interesting class of β-diketones containing a pyrazole fused to a chelating arm. They have applications in pharmaceuticals, dyes, and coordination chemistry [10–12]. Jensen described a direct one-step synthesis method, and his approach was successfully employed for the preparation of various 4-acyl substituted pyrazolones [13]. Expansibility of acylpyrazolones enhance the denticity of these ligands. The expansibility of acylpyrazolones is primarily achieved through a Schiff base reaction as given in Figure 1.1.

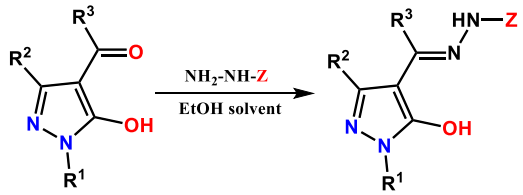

Figure 1.1 Expansion of 4-acyl-5-pyrazolones via Schiff base reaction.

Brief literature review on inner transition metal complexes

The unique feature of neodymium, dysprosium, and terbium metal complexes among all lanthanides lies in their distinct magnetic and luminescent properties, making them particularly valuable for applications in technologies such as magnetic materials, sensors, and optoelectronic devices. In actinide series, thorium and uranium showcasing characteristic chemical properties, including variable oxidation states and complex coordination chemistry.

Complexes of inner transition metals with acylpyrazolones

One of the primary benefits of Acylpyrazolone ligands is their capability to create enduring complexes with a wide range of elements, including main group, transition metals, lanthanides, and actinides, which can be utilized for various purposes. These complexes are known for their synthesis, stability, properties, and coordination modes. Lanthanides and Actinides can exhibit coordination numbers ranging from 6 to 10 when interacting with bidentate acyl-pyrazolone ligands.

Aims and Objectives

The main objective of the Research is synthesis of the acyl pyrazolone ligands and their complexes with some inner transition metals (U, Th, Dy, Nd, Tb, etc.) and their characterization with all available techniques such as IR, NMR, TG-DTA, UV-VIS, Mass, etc. and study their single-crystal structure, fluorescence behaviour, electronic spectra, etc.

Chapter 2: Acylpyrazolone ligands and their Uranyl metal complexes: Synthesis, Characterization and Structural Features.

Chapter 2(a): Synthesis, Characterization and Crystal Features of Bidentate and Tridentate acylpyrazolone ligands.

Synthesis of bidentate ligands

The synthesis of six Ligands (HL^1, HL^2, HL^3, HL^4, HL^5, and HL^6) is mentioned in Figure 2a.1 and they prepared for the complexation process.

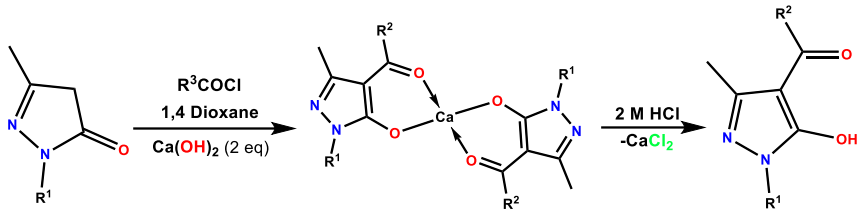

L^1 ligand: R^1 = phenyl, R^2 = p-chlorobenzoyl
L^2 ligand: R^1 = m-chlorophenyl, R^2 = p-chlorobenzoyl
L^3 ligand: R^1 = o-tolyl, R^2 = p-chlorobenzoyl
L^4 ligand: R^1 = phenyl, R^2 = 3,5-dimethylbenzoyl
L^5 ligand: R^1 = m-chlorophenyl, R^2 = 3,5-dimethylbenzoyl
L^6 ligand: R^1 = o-tolyl, R^2 = 3,5-dimethylbenzoyl

Figure 2a.1 Synthesis of bidentate acylpyrazolone ligands.

Physical properties

Property	HL^4		HL^5		HL^6	
Recrystallized in	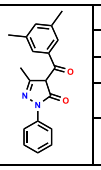	Rectified Spirit	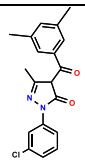	Rectified spirit	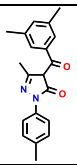	-
Yield		93.34%		89.8%		86.73%
Melting Point		142 °C		110°C		134°C
Mole. Formula		$C_{19}H_{18}N_2O_2$		$C_{19}H_{17}ClN_2O_2$		$C_{20}H_{20}N_2O_2$
Molecular weight		306.14		340.10		320.15

Synthesis of tridentate ligands

Tridentate ligand HL^7 was synthesized using Schiff base reaction to get the tridenticity for complexation with metals (See Figure 2a.2).

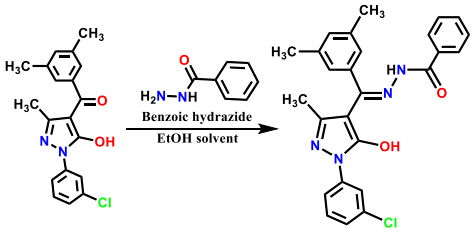

Physical Property	HL^7
Recrystallized in	Rectified Spirit
Yield	93.16%
Melting Point	200 °C
Mole. Formula	$C_{26}H_{23}ClN_4O_2$
Molecular weight	458.95

Figure 2a.2 Synthesis of tridentate acylpyrazolone ligand.

FTIR spectral analysis

Table 2a.1 represents some significant vibrations in HL^4-HL^7 ligands and FTIR spectra for HL^4 ligand is shown in Figure 2a.3.

Table 2a.1 Few significant FTIR vibrations for ligands HL^4-HL^7.

Code	$\nu_{C=O}$ benzoyl	$\nu_{C=O}$ acyl	Cyclic $\nu_{C=N}$	ν_{C-C} aromatic	ν_{N-N}	ν_{C-H}
L^4	1621	1605	1511	1307	1175	1067
L^5	1621	1589	1554	1344	1176	1080
L^6	1622	1607	1511	1356	1175	1066
L^7	1640	1595	1518	1368	1142	1064

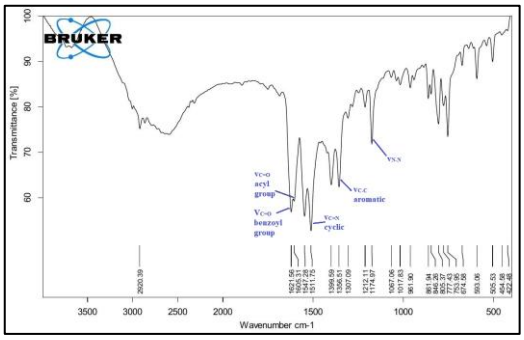

Figure 2a.3 FTIR spectrum of HL^4

Single crystal x-ray and Hirshfeld surface analysis

Figure 2a.4 shows the single crystal x-ray structure of HL^4 ligand. The Hirshfeld surface and energy calculations were performed as given in Figure 2a.5.

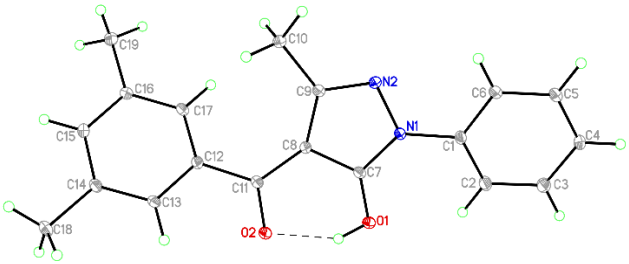

Figure 2a.4 ORTEP diagram for HL^4 ligand.

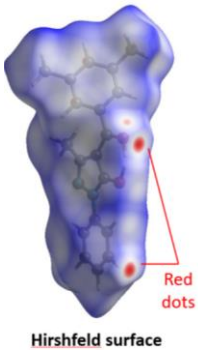

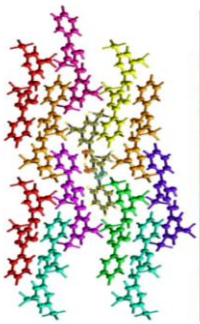

	N	E_{ele}	E_{pol}	E_{dis}	E_{rep}	E_{total}	Lattice energy
	2	-0.6	-0.2	-7.4	2.2	-5.7	-5.7
	2	-18.9	-6.4	-97	45.6	-73.8	-73.8
	2	-3	-1	-19.4	9.8	-13.2	-13.2
	1	-5.4	-3.6	-45.3	22.3	-30.6	-15.3
	2	-3.6	-1.3	-24	12	-16.4	-16.4
	2	-0.9	-0.5	-7.7	2.2	-6.4	-6.4
	2	0	0	-1.8	0	-1.7	-1.7
	1	-0.4	-0.4	-15.7	8.4	-8	-4
	1	-1.3	-0.5	-15.4	5	-11.4	-5.7
	1	0.1	-6.3	-27.3	16.5	-15.3	-7.65
	1	0	0	-2.1	0.1	-1.8	-0.9

Figure 2a.5 Hirshfeld surface and energy calculation in ligand HL^4.

Conclusions

The HL^1-HL^7 bidentate and HL^7 tridentate acylpyrazolone ligands were synthesized and characterized. Structural elucidation using FTIR spectral analysis shows significant vibrations. The single crystal data are largely used to examine their structure, geometry, composition, surface interactions, and lattice energy. The Hirshfeld surface analysis was also carried out to identify the crystal strength through interaction energies and intermolecular non-covalent surface interactions in the ligand.

Chapter 2 (b): Synthesis, Covalency Sequence, and Crystal Features of Pentagonal Uranyl Acylpyrazolone Complexes along with DFT Calculation and Hirshfeld Analysis.

Using HL^1, HL^2, HL^3, and HL^4 ligands, four uranyl complexes (1, 2, 3, and 4, respectively) were synthesized using the following process (Figure 2b.1).

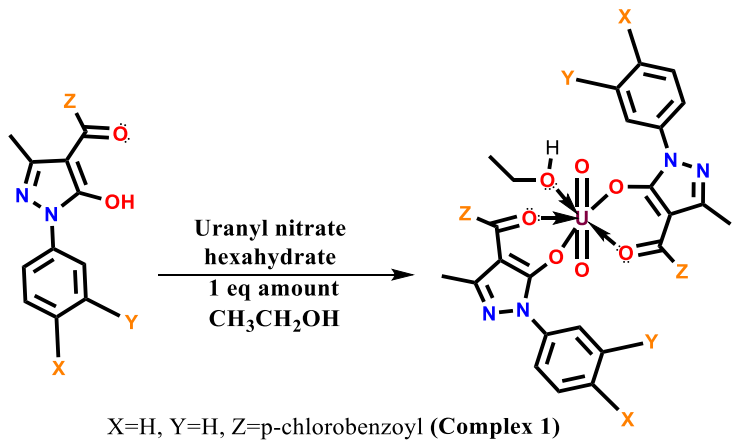

X=H, Y=H, Z=p-chlorobenzoyl **(Complex 1)**
X=H, Y=Cl, Z=p-chlorobenzoyl **(Complex 2)**
X=CH_3, Y=H, Z=p-chlorobenzoyl **(Complex 3)**
X=H, Y=H, Z=3,5-dimethylbenzoyl **(Complex 4)**

U-complex

Figure 2b.1 Synthetic route for uranyl complexes.

FTIR spectral analysis

The FTIR spectral analysis gives primary idea about complex formation by observing decline in the $\nu_{C=O\ (benzoyl)}$ and $\nu_{C=O\ (acyl)}$ peak values in complexes compare to similar bands in the ligands. This comparative analysis is provided in Table 2b.1 and Figure 2b.2 shows the FTIR spectrum of complex 4. The covalency sequence of four complexes (2>3>1>4) is nearly in the reverse order of the U=O ν_{as} and ν_{s} vibrations (4>1>3>2).

Table 2b.1 The comparative FTIR spectral analysis of complexes 1, 2, 3, and 4.

Code	$\nu_{C=O}$ benzoyl	$\nu_{C=O}$ acyl	Cyclic $\nu_{C=N}$	ν_{C-H}	ν_{as} (U=O)	ν_{s} (U=O)
HL[4]	1621	1605	1511	1067	-	-
Complex 1	1577	1557	1472	1013	920	833
Complex 2	1591	1557	1471	1089	863	778
Complex 3	1591	1558	1436	1089	912	823
Complex 4	1618	1602	1480	1062	925	808

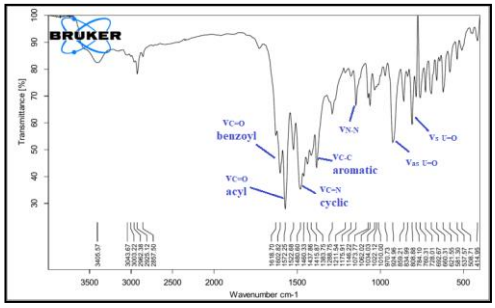

Figure 2b.2 FTIR spectrum of complex 4.

Electronic spectral analysis

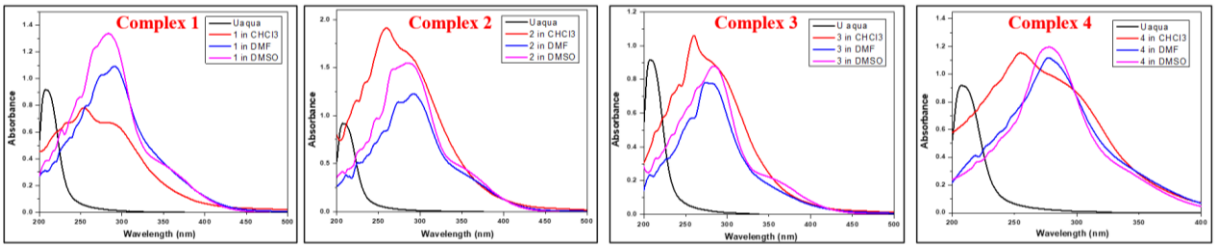

Figure 2b.3 The electronic spectra of complexes 1-4.

The electronic spectra of complexes 1-4 were taken in 10^{-6} M solutions of different solvents, which are provided in Figure 2b.3. Sinha's covalency parameters for different solvents were calculated from these electronic spectra (Table 2b.2), indicate a small amount of relative covalent character (DMSO>DMF>$CHCl_3$) in the case of Uranium complexes.

Table 2b.2 Sinha's covalency parameters for complexes 1-4 in different solvents.

Complex	**1**	**2**	**3**	**4**	**1**	**2**	**3**	**4**	**1**	**2**	**3**	**4**
Solvent	**$CHCl_3$**				**DMF**				**DMSO**			
ν_{comp} (nm)	253.9	261.09	260.03	255.0	290.5	291.7	284	277.1	283.8	283	283	277.8
$\delta = \frac{1-\beta}{\beta}$	-0.180	-0.200	-0.202	-0.185	-0.286	-0.286	-0.270	-0.250	-0.27	-0.265	-0.265	-0.252

Single crystal x-ray diffraction analysis

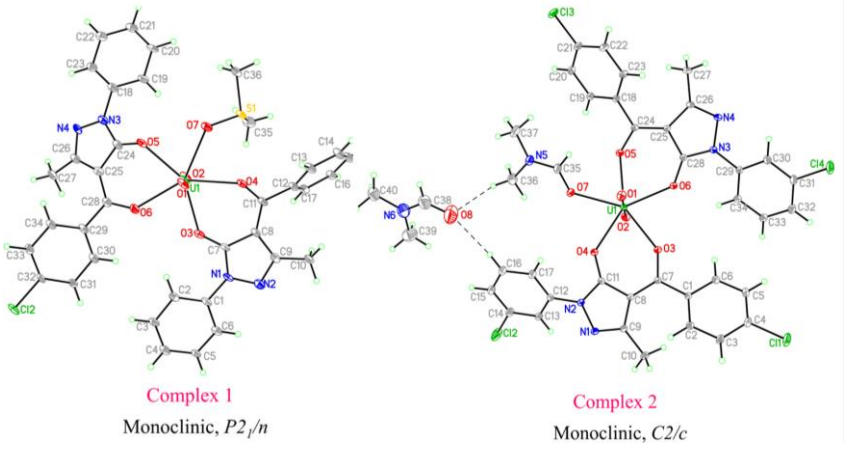

Complex 1
Monoclinic, $P2_1/n$

Complex 2
Monoclinic, $C2/c$

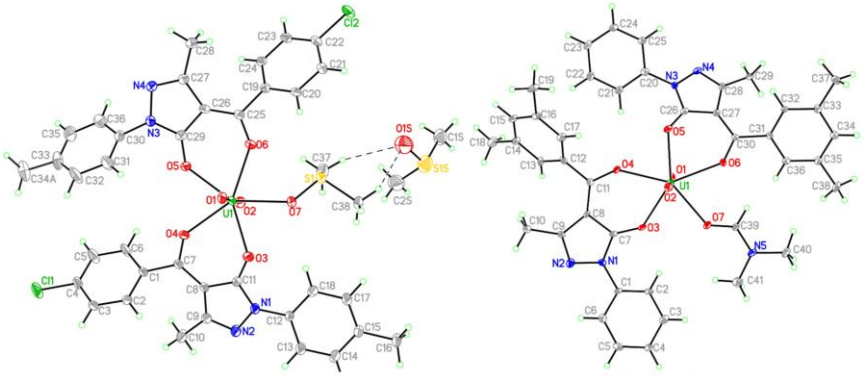

Figure 2b.4 Single-crystal ORTEP diagram for complexes 1-4.

Figure 2b.4 shows the single crystal x-ray structure of complexes 1-4 with their crystal system and space groups. In all complexes, U-O bond lengths of acyl O-atoms are slightly higher than pyrazolone O-atoms. The covalency order for complexes was found 2>3>1>4, which is impacted by values of stretching frequencies, values of average bond lengths on the pentagonal equatorial plane, average bond lengths of axial uranyl bonds, solvent coordination on the fifth site of a pentagonal plane, and type of aryl group on the nitrogen of pyrazolone ring.

DFT computational analysis

The geometry of complexes 1-4 were optimized using B3LYP/SDD basis sets. Higher HOMO-LUMO energy bandgap shows greater stability and higher covalency. Based on this, greater covalency of complex 2 was proved. Moreover, using energy bandgap value, global index parameters were calculated [14] (Table 2b.3). The HOMO-LUMO energy bandgap calculations are provided in Figure 2b.5.

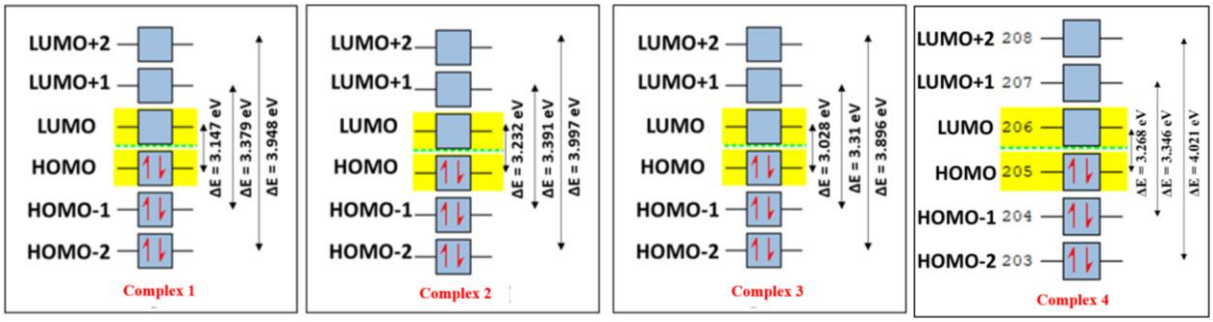

Figure 2b.5 HOMO-LUMO energy gap for complexes 1-4.

Table 2b.3 Global index parameters for complexes 1-4.

Properties of complex	Mathematical Formula	Complex 1	Complex 2	Complex 3	Complex 4
E_{HOMO}	E_{HOMO}	-5.87	-6.209	-5.697	-5.738
E_{LUMO}	E_{LUMO}	-2.723	-2.977	-2.669	-2.470
ΔE	$\Delta E = E_{LUMO} - E_{HOMO}$	3.147	3.232	3.028	3.268
Ionization potential (IP)	$IP = -E_{HOMO}$	5.87	6.209	5.697	5.738
Chemical Potential (μ)	$\mu = \frac{1}{2}(E_{HOMO} + E_{LUMO})$	-4.2965	-4.593	-4.183	-4.104
Electron affinity (EA)	$EA = -E_{LUMO}$	2.723	2.977	2.669	2.470
Electronegativity (EN)	$EN = -\frac{1}{2}(E_{HOMO} + E_{LUMO})$	4.2965	4.593	4.183	4.104
Global Hardness (Ƞ)	$\eta = -\frac{1}{2}(E_{HOMO} - E_{LUMO})$	1.5735	1.616	1.514	1.634
Softness (S)	$S = \frac{1}{2\eta}$	0.3177	0.3094	0.3302	0.306
Electrophilicity index (ω)	$\omega = \frac{\mu^2}{2\eta}$	5.8659	6.5271	5.7785	5.154

Hirshfeld surface area analysis

Using the crystal explorer 17.5 programme, the donor-acceptor interaction sites and intermolecular interactions with neighbouring molecules can be visualised for all four complexes. Figure 2b.6 and 2b.7 shows the Hirshfeld surface and its percentage interactions with neighbouring molecules.

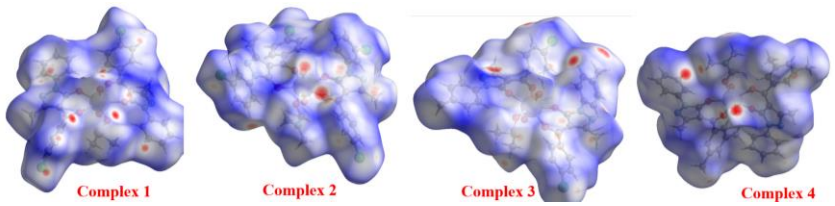

Figure 2b.6 The Hirshfeld surface for complexes 1-4.

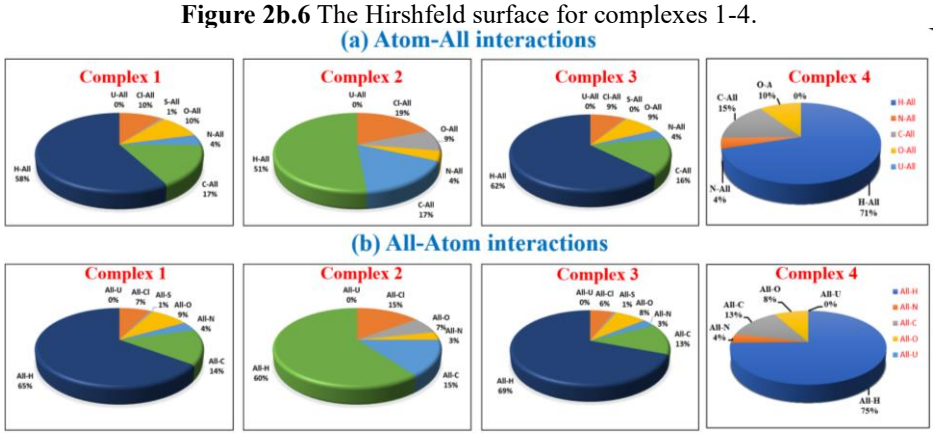

Figure 2b.7 The percentage interaction of Hirshfeld surface with neighbouring atoms in complexes 1-4.

Conclusions

Four pentagonal bipyramidal uranyl complexes were synthesized and characterized using acylpyrazolone ligands. The characterized data are largely used to examine their structure, geometry, composition, surface interactions, and covalency sequence. Electronic spectral studies were carried out to calculate Sinha's covalency parameters to get covalency order in different solvents.

Chapter 2 (c): Uranyl(VI) Mixed-ligand complex synthesis and characterization using 4-acylhydrazone-5-pyrazolone and 4-acylpyrazolone: Covalency, crystal assay, DFT study and Hirshfeld analysis.

Experimental work

Using 1:1 ethanolic mixture of HL^5 and HL^7 ligands in equivalent amount, a mixed ligand complex (complex 5) was synthesized (See Figure 2c.1).

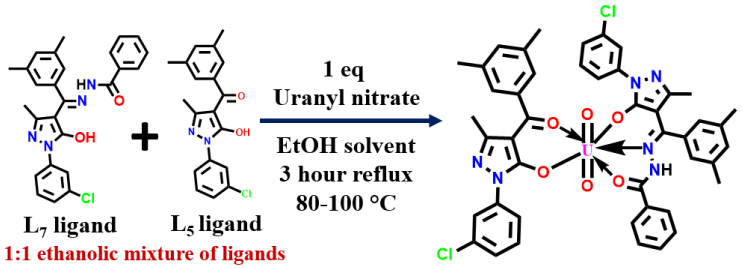

Property	Complex 5
Yield	92.72%
Melting Point	>200 °C
Mole. Formula	$C_{45}H_{38}Cl_2N_6O_6U$
Molecular weight	1067.76
Recrystallized in	EtOH
Λ^o_M (ohm^{-1} cm^{2}mol^{-1})	4.23

Figure 2c.1 Synthetic route of mixed ligand uranyl acylpyrazolone complex with physical properties.

FTIR spectral analysis

Table 2c.1 The comparative FTIR spectral analysis of complexes 1, 2, 3, and 4.

Code	$\nu_{C=O}$ benzoyl	$\nu_{C=O}$ acyl	Cyclic $\nu_{C=N}$	ν_{C-H}	ν_{as} (U=O)	ν_s (U=O)
HL^5	1621	1589	1554	1344	-	-
HL^7	1640	1595	1518	1368	-	-
Complex 5	1600	1557	1476	1374	914	776

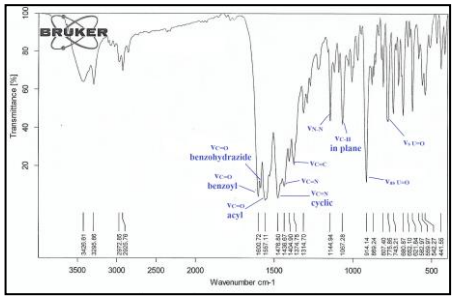

Figure 2c.2 FTIR spectrum of complex 5.

As observed earlier, decrease in the $\nu_{C=O\ (benzoyl)}$ and $\nu_{C=O\ (acyl)}$ peak values in complexes compare to similar bands in the ligands suggest complex formation. This comparative analysis is provided in Table 2c.1 and Figure 2c.2 shows the FTIR spectrum of complex 5.

Single crystal x-ray diffraction analysis

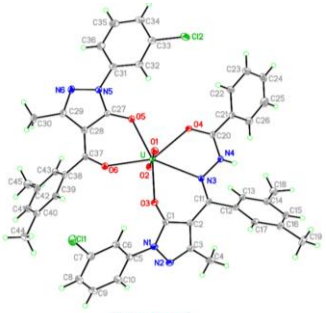

Figure 2.14 single crystal ORTEP diagram for complex 5.

Figure 2.14 shows the single crystal x-ray structure of complex 5 with its crystal system and space group.

In complex 5, U-O bond lengths of acyl O-atoms are slightly higher than pyrazolone O-atoms.

The covalency could be impacted by values of stretching frequencies, values of average bond lengths on the pentagonal equatorial plane, average bond lengths of axial uranyl bonds, solvent coordination on the fifth site of a pentagonal plane, and type of aryl group on the nitrogen of pyrazolone ring.

DFT computational analysis

The geometry of complex 5 was optimized using B3LYP/SDD basis set.

Based on HOMO-LUMO energy bandgap value, global index parameters were calculated [14] (Table 2c.2).

The HOMO-LUMO energy bandgap calculations are provided in Figure 2c.3.

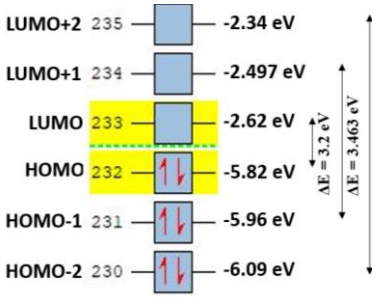

Figure 2c.3 HOMO-LUMO energy gap in complex 5.

Table 2c.2 Global index parameters for complex 5.

Parameters	Mathematical Formula	Uranyl complex
E_{LUMO}	E_{LUMO}	-2.62
E_{HOMO}	E_{HOMO}	-5.82
ΔE	$\Delta E = E_{LUMO} - E_{HOMO}$	3.2
Electron affinity (EA)	$EA = -E_{LUMO}$	2.62
Ionization potential (IP)	$IP = -E_{HOMO}$	5.82
Chemical Potential (μ)	$\mu = ½ (E_{Homo} + E_{Lumo})$	-4.22
Global Hardness (η)	$\eta = - ½ (E_{Homo} - E_{Lumo})$	1.6
Softness (S)	$S = 1/2\eta$	0.312
Electronegativity (EN)	$EN = -½ (E_{Homo} + E_{Lumo})$	4.22
Electrophilicity index (ω)	$\omega = \mu^2/2\eta$	5.556

Hirshfeld surface area analysis

Using the crystal explorer 17.5 programme, the donor-acceptor interaction sites and intermolecular interactions with neighbouring molecules can be visualised for complex 5. Figure 2c.4 shows the Hirshfeld surface and its percentage interactions with neighbouring molecules.

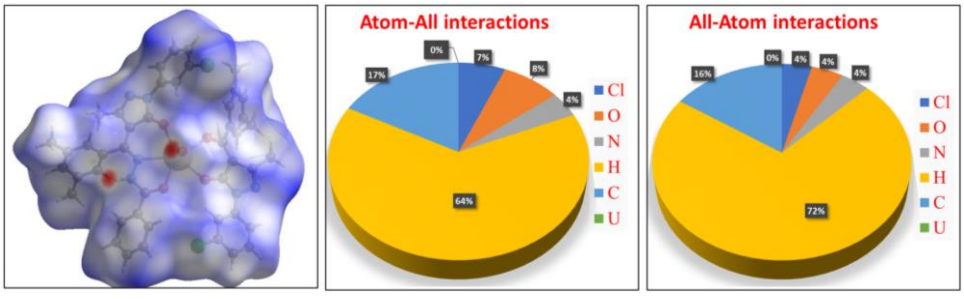

Figure 2c.4 Hirshfeld surface and its percentage interactions in complex 5.

Electronic spectral analysis

The electronic spectra of complex 5 was taken in 10^{-6} M solutions of different solvents, which is provided in Figure 2c.5. Sinha's covalency parameters for different solvents were calculated from the electronic spectra (Table 2c.3). There is no solvent binding to the equatorial pentagonal position as seen in uranyl acylpyrazolone complexes; therefore, the trend of covalent character in all solvents remains nearly the same.

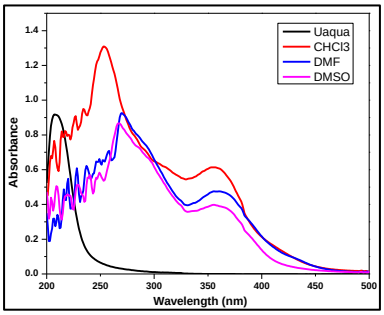

Figure 2c.5 Electronic spectra of complex 5.

Table 2c.3 Sinha's covalency parameter calculation for complex 5.

Solvent	ν_{comp} value (in nm)	$\delta = \frac{1-\beta}{\beta}$
$CHCl_3$	355.3	0.714
DMF	355.6	0.715
DMSO	354.9	0.712

Conclusions

Mixed-ligand pentagonal bipyramidal uranyl complex was synthesized and characterized using acylpyrazolone ligands. The characterized data are largely used to examine their structure, geometry, composition, surface interactions, and covalency sequence. Electronic spectral studies were carried out to calculate Sinha's covalency parameters to get covalency order in different solvents.

Chapter 3 Acylpyrazolone ligands and their Neodymium metal complexes: Synthesis, Characterization and Structural Features.

Chapter 3 (a) Structural Features, Emission Analysis, and Covalency Comparison of Neodymium Acylpyrazolone Complexes using Oscillator Strengths, Covalency and Judd-Ofelt Parameters.

Experimental work

3 eq ethanolic solution of ligand and 3 eq $NaOH_{(aq)}$ was stirred for a half-hour at 80–100 °C as shown in Figure 3a.1. Then, dropwise additions of 1 eq ethanolic neodymium(III) nitrate hexahydrate solution were made. After 18 hours of refluxing, the solution was transferred to a container where it was slowly evaporated to produce an eight-coordinated neodymium-acylpyrazolone complex.

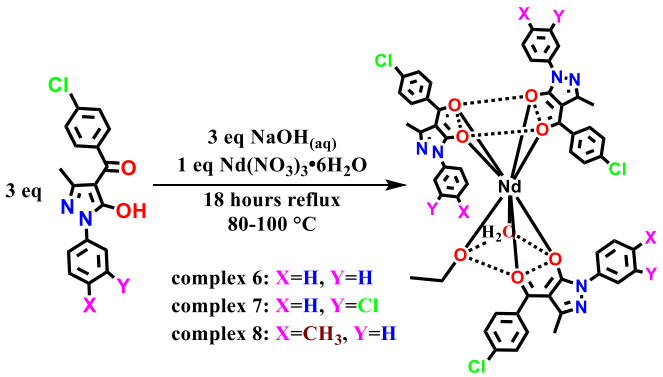

Property	Complex 6	Complex 7	Complex 8
Yield	93.14%	95.24%	92.66%
Melting Point	>200 °C	>200 °C	>200 °C
Mole. Formula	$C_{53}H_{43}Cl_3N_6NdO_8$	$C_{53}H_{40}Cl_6N_6NdO_8$	$C_{56}H_{49}Cl_3N_6NdO_8$
Molecular weight	1142.55	1245.88	1184.63
Recrystalized in	EtOH	-	-
Λ^o_M (ohm^{-1} cm^2mol^{-1})	10	5	4

Figure 3a.1 Synthetic route for complexes 6, 7, and 8.

FTIR spectral analysis

The significant observation is decrease in the $\nu_{C=O\ (benzoyl)}$ and $\nu_{C=O\ (acyl)}$ peak values in complexes compare to similar bands in the ligands (Table 3a.1). FTIR spectrum of complex 6 is given in Figure 3a.2.

Table 3a.1 The comparative FTIR spectral analysis of complexes 6-8.

Vibrations [cm^{-1}]	L_1	Complex 6	L_2	Complex 7	L_3	Complex 8
$\nu_{(C=O)}$ benzoyl	1620	1612	1624	1612	1694	1615
$\nu_{(C=O)}$ acyl	1590	1592	1590	1589	1601	1599
cyclic $\nu_{(C=N)}$	1484	1475	1484	1478	1446	1475

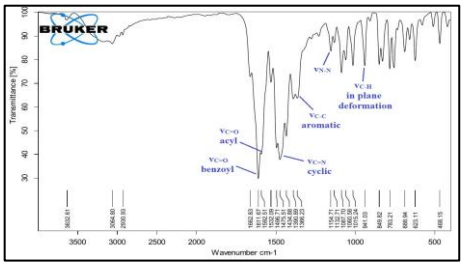

Figure 3a.2 FTIR spectrum of complex 6.

Single crystal x-ray diffraction analysis

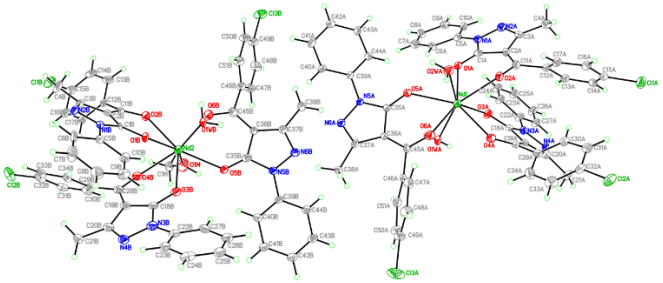

Figure 3a.3 ORTEP diagram for complex 6.

Figure 3a.3 shows the single crystal x-ray structure of complex 6 with its crystal system and space group.

In complex 6, The lengths of the C-O bonds in the acyl group are slightly higher than typical for C–O distance in ketones (1.23 Å) due to O→Nd bonding.

Powder XRD analysis

The stimulated pattern matches well with the experimental pattern for all three complexes (Figure 3a.4). This confirms that all the complexes have similar geometry and structure.

This also ensures the structure obtained from a single crystal represents the bulk of the complexes.

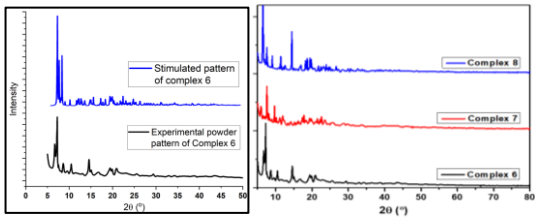

Figure 3a.4 Stimulated pattern of complex 6 and powder XRD plots for complexes 6-8.

Absorption and emission spectral analysis

Electronic spectra of 0.01 M solution of complexes 6, 7, and 8 in various solvents were recorded (Figure 3a.5). There are seven transitions ($^4F_{3/2}$→$^4I_{9/2}$, $^4F_{5/2}$→$^4I_{9/2}$, $^4F_{7/2}$→$^4I_{9/2}$, $^4F_{9/2}$→$^4I_{9/2}$, $^4G_{5/2}$→$^4I_{9/2}$, $^4G_{7/2}$→$^4I_{9/2}$, and $^4G_{9/2}$→$^4I_{9/2}$). The transitions $^4G_{5/2}$, $^4G_{7/2}$→$^4I_{9/2}$ are **Hypersensitive transitions** as they exhibits a distinctive sensitivity to the ligand surrounding the Nd(III) ion.

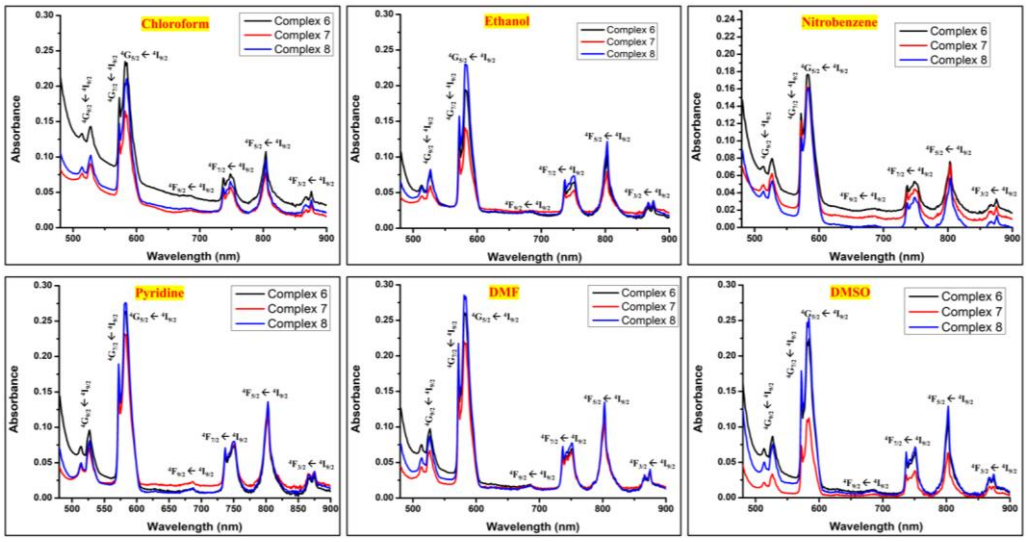

Figure 3a.5 Electronic spectra of 0.01 M solution of complexes 6, 7, and 8 in various solvents.

The spectral strength of the absorption band is described by oscillator strengths (P)[15], which have been experimentally connected to the integral area of the absorption band and can be written as

$$\mathbf{f_{exp}\ or}\ P = 4.31 \times 10^{-19} \left[\frac{9\eta}{\eta^2+2}\right] \int \varepsilon_{max}(\bar{\nu})d\bar{\nu}$$

Moving from the $Nd^{3+}_{aqua-ion}$ to the complex across all the utilised solvents raises the oscillator strength of $^4G_{5/2} \leftarrow {}^4I_{9/2}$ transition by a factor of 4 to 6 times (**Hypersensitive**). The intensity of the 4f-4f electric dipole is particularly well-promoted by pyridine in both the complexes 6 and 8. The intensification is typically observed in the order: Pyridine > DMF > DMSO > Ethanol > chloroform > Nitrobenzene. The influence of covalency in terms of the Judd-Ofelt parameters (Ω_2, Ω_4, Ω_6) can be described by the following equation (See Table 3a.2)

$$f_{ed} = \frac{8\pi^2 mc\sigma}{3h(2J+1)} \cdot x \sum_{\lambda=2,4,6} \Omega_\lambda |\langle a \| U^\lambda \| b \rangle|^2$$

Table 3a.2 Judd-Ofelt intensity parameters for complexes 6, 7, and 8.

Complex	J-O Parameter [$\Omega/10^{-20}$ cm^2]	Chloroform	Ethanol	Nitrobenzene	Pyridine	DMF	DMSO
6	Ω_2	5.07	5.46	5.17	7.96	7.74	6.61
	Ω_4	1.88	1.45	1.16	2.11	1.72	1.69
	Ω_6	3.92	4.63	3.36	6.19	5.94	5.33
7	Ω_2	3.87	4.22	4.86	6.76	6.32	7.20
	Ω_4	1.68	1.37	1.46	2.06	2.19	1.50
	Ω_6	3.28	2.87	3.64	5.72	4.97	6.52
8	Ω_2	5.36	6.60	5.27	8.65	7.96	7.66
	Ω_4	1.51	1.92	1.56	2.29	2.68	2.23
	Ω_6	3.96	5.55	3.44	6.89	2.16	5.92

To demonstrate the covalency of complexes 6, 7, and 8, Nephelauxetic ratio (β), Sinha parameter (δ%), bonding parameter (b1/2), and angular overlap parameter (η) were calculated using following equations.

$$\text{Nephelauxetic ratio } \beta = \frac{\bar{\nu}_{complex}}{\bar{\nu}_{free\ ion}} \qquad \text{Bonding parameter } b^{\frac{1}{2}} = \left(\frac{1-\beta}{2}\right)^{1/2}$$

$$\text{Sinha parameter } \delta\% = \left[\frac{1-\beta}{\beta}\right] \times 100 \qquad \text{Angular overlap parameter } \eta = \frac{1-\sqrt{\beta}}{\sqrt{\beta}}$$

Using solid-state emission spectra of complexes 6-8 (Figure 3a.6), the spectral strength (f_{exp} or P) and Judd-Ofelt parameters (Ω_t) were once more computed and "Antenna effect" energy diagram was studied.

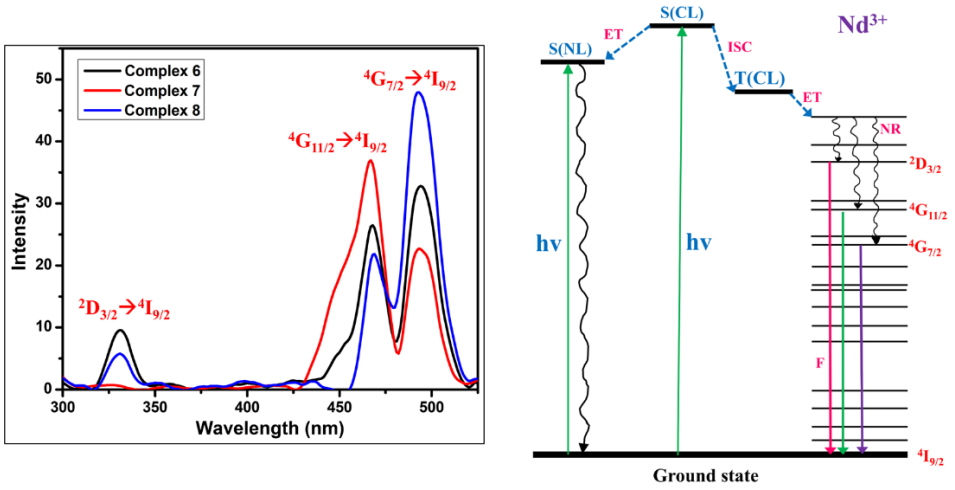

Figure 3a.6 Solid state emission spectra and antenna effect energy diagram for complexes 6-8.

Conclusions

The main goals of the present research aimed to (a) measure the hypersensitive transition peak intensity of Nd(III)-acylpyrazolone complexes across different solvents, (b) show how the hypersensitive transition (oscillator strength, band shapes, and Judd-Ofelt parameters) responds to structural variations between the ligand in several complexes, (c) show the impact of various coordinating and non-coordinating solvents, (d) Calculate the degree of covalency using various covalency parameters.

Chapter 3 (b) Neodymium based acylpyrazolone complexes: Synthesis and physicochemical characterizations.

Experimental work

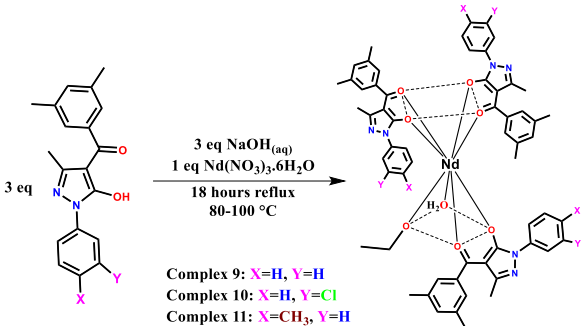

Property	Complex 9	Complex 10	Complex 11
Yield	96.87%	93.01%	95.34%
Melting Point	223-230 °C	212-220 °C	208-215 °C
Mole. Formula	$C_{59}H_{58}N_6NdO_8$	$C_{59}H_{55}Cl_3N_6NdO_8$	$C_{62}H_{64}N_6NdO_8$
Molecular weight	1123.39	1226.72	1163.39
Recrystalized in	-	EtOH	-
Λ°_{M}	11	7	9

Figure 3b.1 Synthetic route for complexes 9, 10, and 11.

FTIR spectral analysis

The significant observation is decrease in the $\nu_{C=O\ (benzoyl)}$ and $\nu_{C=O\ (acyl)}$ peak values in complexes compare to similar bands in the ligands (Table 3b.1). FTIR spectrum of complex 10 is given in Figure 3b.2.

Table 3b.1 FTIR spectral analysis of complexes 9-11.

Vibrations [cm^{-1}]	L_4	Complex 9	L_5	Complex 10	L_6	Complex 11
$\nu_{(C=O)}$ benzoyl	1621	1611	1624	1614	1622	1596
$\nu_{(C=O)}$ acyl	1605	1580	1589	1587	1607	1577
cyclic $\nu_{(C=N)}$	1511	1483	1554	1480	1511	1486
$\nu_{aromatic(C-C)}$	1307	1370	1344	1363	1356	1383
$\nu_{(N-N)}$	1175	1141	1176	1131	1175	1146

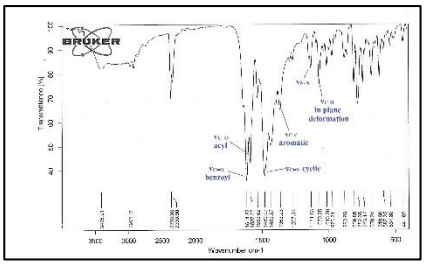

Figure 3b.2 FTIR spectrum of complex 10.

Single crystal x-ray diffraction analysis

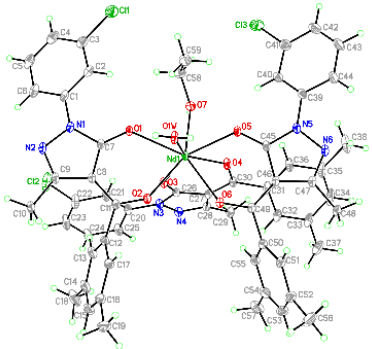

Figure 3b.3 ORTEP diagram for complex 10.

Figure 3b.3 shows the single crystal x-ray structure of complex 10 with its crystal system and space group.

In complex 10, The lengths of the C-O bonds in the acyl group are slightly higher than typical for C–O distance in ketones (1.23 Å) due to O→Nd bonding.

Powder XRD analysis

The stimulated pattern matches well with the experimental pattern for all three complexes (Figure 3b.4). This confirms that all the complexes have similar geometry and structure.

This also ensures the structure obtained from a single crystal represents the bulk of the complexes.

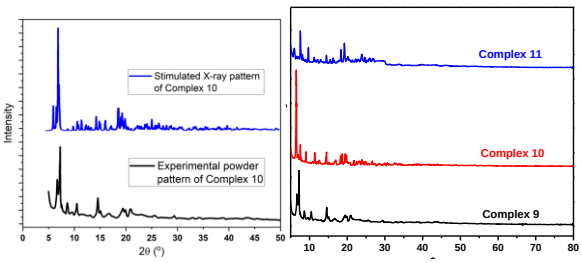

Figure 3b.4 Stimulated pattern of complex 8 and powder XRD plots for complexes 9-11.

Absorption and emission spectral analysis

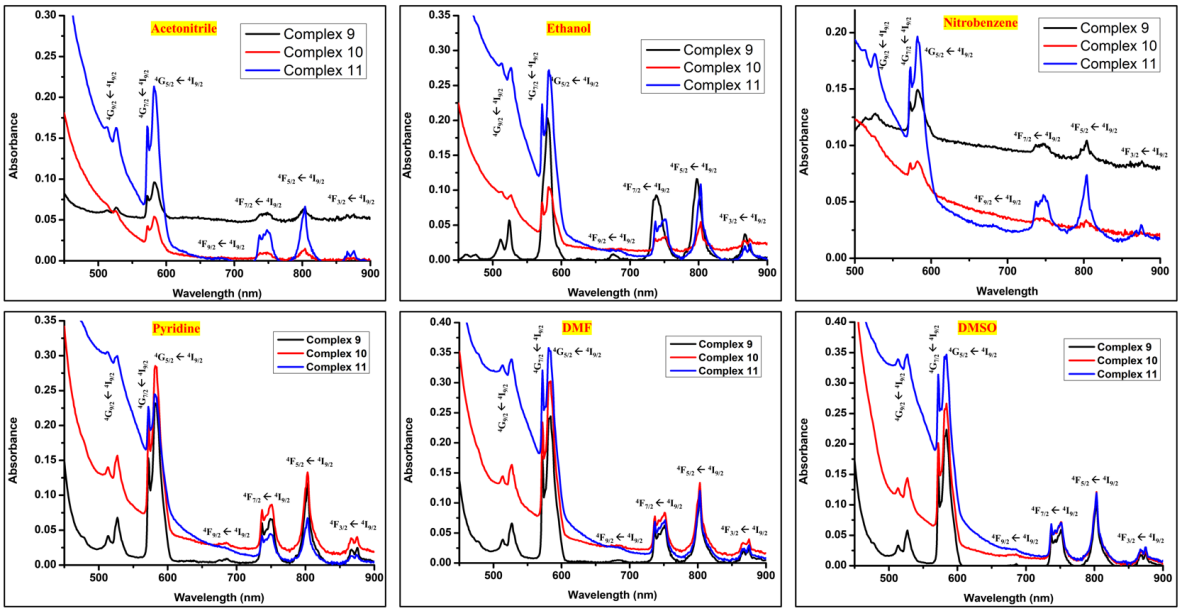

Figure 3b.5 Electronic spectra of 0.01 M solution of complexes 9, 10, and 11 in various solvents.

The spectral strength of the absorption band is described by oscillator strengths (P), intensity of hypersensitivity, and the influence of covalency in terms of the Judd-Ofelt parameters (Ω_2, Ω_4, Ω_6) were analysed using formula as mentioned in earlier chapter. The covalency parameters also calculated using electronic spectra (Figure 3b.5). From solid-stae emission spectra of Figure 3b.6, "Antenna effect" energy diagram was examined.

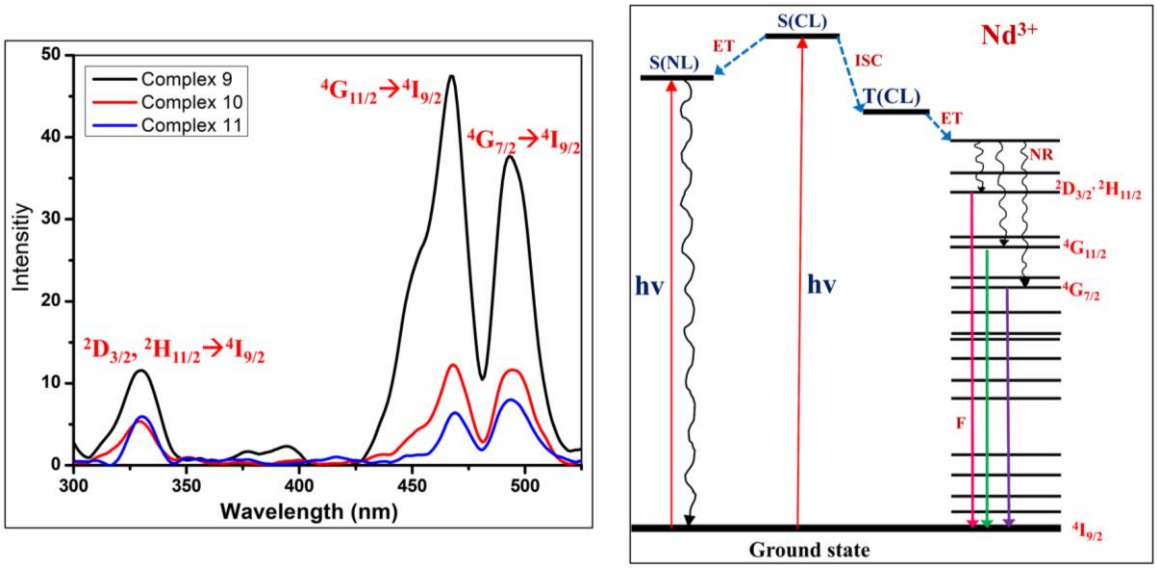

Figure 3b.6 Solid state emission spectra and antenna effect energy diagram for complexes 9-11.

Conclusions

Three neodymium-acylpyrazolone complexes—9, 10, and 11—had eight-coordinated distorted square antiprism geometry, which was held in space by three σ-donating acylpyrazolone ligands, one water molecule, and one ethanol molecule. The intensity of the hypersensitive transitions of chemically associated Nd(III)-acylpyrazolone complexes as well as pseudo-hypersensitive transitions across different solvents was measured. Oscillator strength, band shapes, covalency parameters, and Judd-Ofelt parameters were calculated to study covalent character.

Chapter 4 Dysprosium Acylpyrazolone complexes: Synthesis, Structural Features, Fluorescence and Electronic properties.

Experimental work

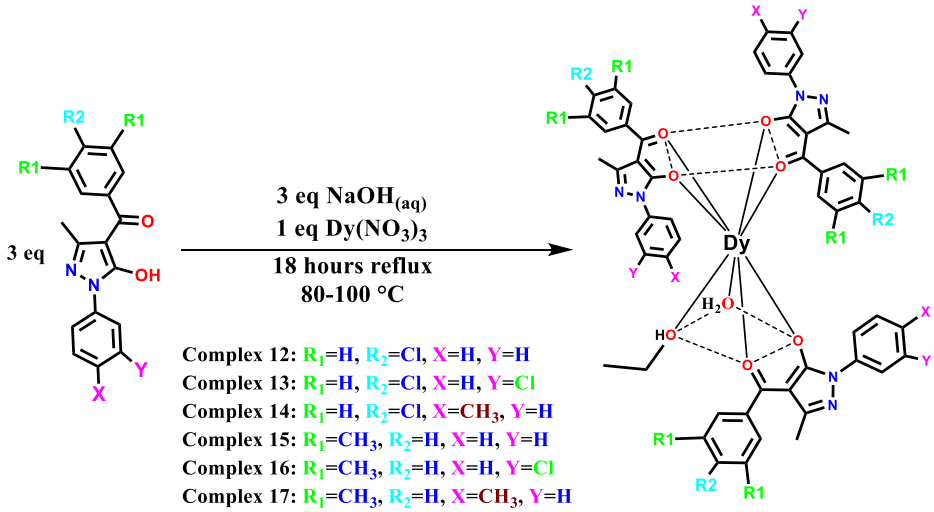

Complex 12: R_1=H, R_2=Cl, X=H, Y=H
Complex 13: R_1=H, R_2=Cl, X=H, Y=Cl
Complex 14: R_1=H, R_2=Cl, X=CH_3, Y=H
Complex 15: R_1=CH_3, R_2=H, X=H, Y=H
Complex 16: R_1=CH_3, R_2=H, X=H, Y=Cl
Complex 17: R_1=CH_3, R_2=H, X=CH_3, Y=H

Figure 4.1 Synthetic route for complexes 12-17.

FTIR spectral analysis

The significant observation is decrease in the $\nu_{C=O\ (benzoyl)}$ and $\nu_{C=O\ (acyl)}$ peak values in complexes compare to similar bands in the ligands (Table 4.1). FTIR spectrum of complex 15 is given in Figure 4.2.

Table 4.1 FTIR spectral analysis of complexes 12-17.

Vibrations [cm^{-1}]	L_1	Complex 12	L_2	Complex 13	L_3	Complex 14	L_4	Complex 15	L_5	Complex 16	L_6	Complex 17
$\nu_{(C=O)}$ benzoyl	1620	1612	1624	1613	1694	1601	1621	1613	1624	1615	1622	1619
$\nu_{(C=O)}$ acyl	1590	1592	1590	1589	1601	1504	1605	1581	1589	1588	1607	1597
cyclic $\nu_{(C=N)}$	1484	1498	1484	1479	1446	1480	1511	1488	1554	1480	1511	1489
$\nu_{aromatic(C-C)}$	1357	1371	1348	1366	1381	1378	1307	1370	1344	1365	1356	1372
$\nu_{(N-N)}$	1213	1155	1210	1158	1178	1159	1175	1134	1176	1135	1175	1147

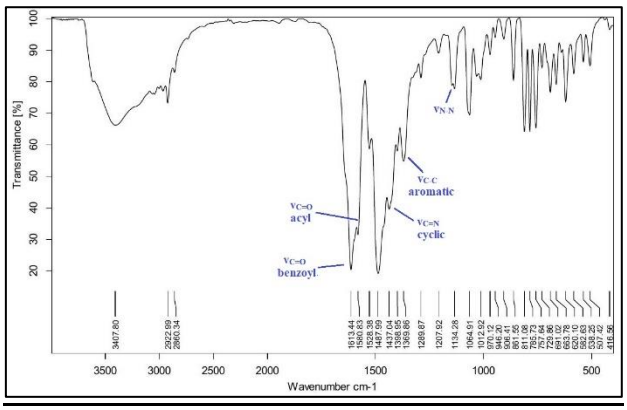

Figure 4.2 FTIR spectrum of complex 15.

Single crystal x-ray diffraction analysis

Figure 4.3 shows the single crystal x-ray structure of complex 15 having orthorhombic crystal system and *P c a 21* space group. In complex 15, The lengths of the C-O bonds in the acyl group are slightly higher than typical for C–O distance in ketones (1.23 Å) due to O→Dy bonding. In comparison to Dy-O(acyl) bond lengths (2.381-2.421 Å), Dy-O(pyrazolone) bond lengths (2.344-2.383 Å) are slightly higher, indicating stronger covalency caused by the acyl group O-atoms. This is because longer bonds lead to a drop in the average bond order between dysprosium and O-atoms, which rises covalency. The stimulated pattern matches well with the experimental pattern for all three complexes (Figure 4.4).

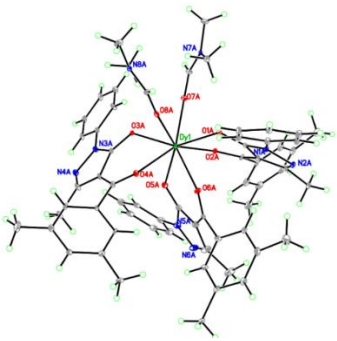

Figure 4.3 ORTEP diagram for complex 15.

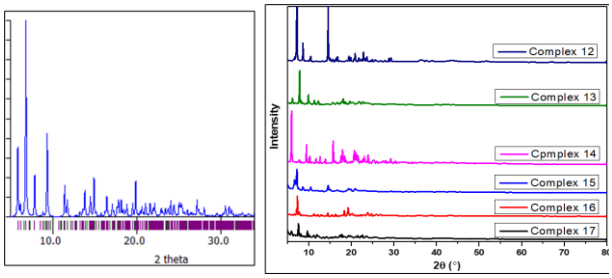

Figure 4.4 Stimulated XRD pattern of complex 15 and powder XRD patterns of complexes 12-17

Fluorescence emission spectral analysis

From the solid-state emission spectra (Figure 4.5), "antenna effect" energy diagram was examined for all complexes. $^4F_{9/2}$→$^6H_{15/2}$ and $^4F_{9/2}$→$^6H_{13/2}$ transitions observed in the blue and yellow zone, respectively. For complexes 12–17 respectively, the Y/B (yellow to blue) ratio was found to be 1.58, 2.72, 1.35, 1.87, 4.11, and 3.22, and it is greater than unity (Y/B>1), indicating an increased level of Dy-O covalency.

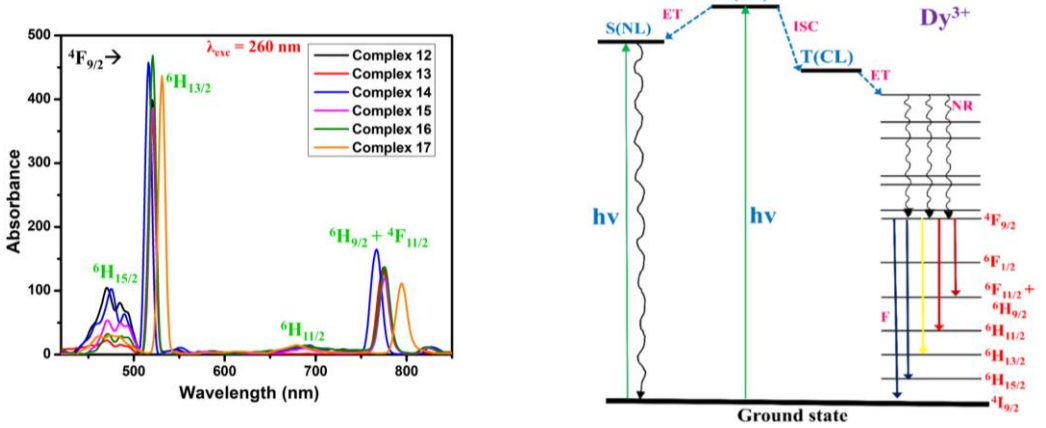

Figure 4.5 The solid-state emission spectra and "Antenna effect" energy diagram for complexes 12–17.

Conclusions

Six Dysprosium-acylpyrazolone complexes—12, 13, 14, 15, 16, and 17—with eight-coordinated distorted square antiprism geometry were synthesized and characterized. Four transitions, their type, and Y/B ratio corresponding to different regions have been examined from the solid-state emission spectra. The transitions $^4F_{9/2}$→$^6H_{15/2}$ and $^4F_{9/2}$→$^6H_{13/2}$ are observed in the blue and yellow regions, respectively, and their Y/B ratio is greater than unity (Y/B>1), indicating an increased level of Dy-O covalency.

Chapter 5 Terbium Acylpyrazolone complexes: Synthesis, Structural Features, Fluorescence and Electronic properties.

Experimental work

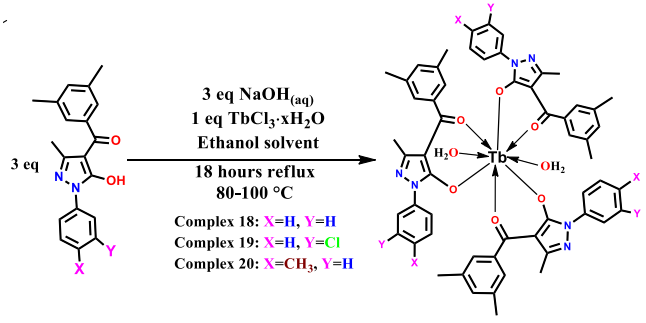

Property	Complex 18	Complex 19	Complex 20
Yield	90.19%	91.41%	84.90%
Melting Point	>200 °C	212-220 °C	208-215 °C
Mole. Formula	$C_{57}H_{52}N_6O_8Tb$	$C_{57}H_{52}N_6Cl_3O_8Tb$	$C_{60}H_{61}N_6O_8Tb$
Molecular weight	1111.03	1214.35	1153.11
Λ^o_M	3.91	4.03	3.64

Figure 5.1 Synthetic route for complexes 18-20.

FTIR spectral analysis

The significant observation is decrease in the $\nu_{C=O\ (benzoyl)}$ and $\nu_{C=O\ (acyl)}$ peak values in complexes compare to similar bands in the ligands (Table 5.1). FTIR spectrum of complex 20 is given in Figure 5.2.

Table 5.1 FTIR spectral analysis of complexes 18-20.

Vibrations [cm^{-1}]	L_4	Complex 18	L_5	Complex 19	L_6	Complex 20
$\nu_{(C=O)}$ benzoyl	1621	1617	1624	1616	1622	1620
$\nu_{(C=O)}$ acyl	1605	1596	1589	1588	1607	1601
cyclic $\nu_{(C=N)}$	1511	1492	1554	1480	1511	1494
$\nu_{aromatic(C-C)}$	1307	1369	1344	1363	1356	1369
$\nu_{(N-N)}$	1175	1145	1176	1145	1175	1145

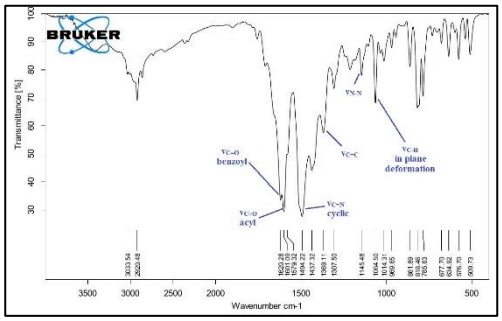

Figure 5.2 FTIR spectrum of complex 20.

Single crystal x-ray diffraction and powder XRD analysis

Figure 5.3 shows the single crystal x-ray structure of complex 20 having triclinic crystal system and *P -1* space group. The stimulated pattern matches well with the experimental pattern for all three complexes (Figure 5.4).

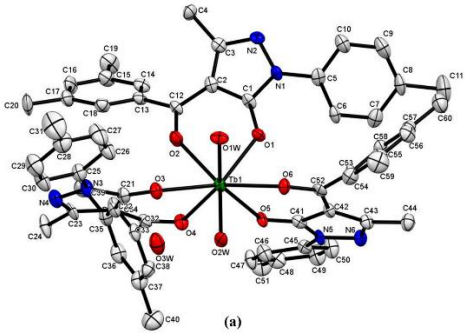

Figure 5.3 ORTEP diagram for complex 20.

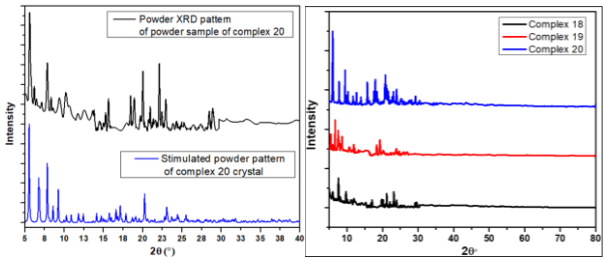

Figure 5.4 Stimulated XRD pattern of complex 20 and powder XRD patterns of complexes 18-20.

Fluorescence emission spectral analysis

From the solid-state emission spectra (Figure 5.5), "antenna effect" energy diagram was examined for all complexes. $^5D_4 \rightarrow {}^7F_6$ and $^5D_4 \rightarrow {}^7F_5$ transitions observed in the blue and green zone, respectively. For complexes 18–20 respectively, the G/B (Green to Blue) ratio was found to be 3.70, 4.15, and 3.37, and it is greater than unity (G/B>1), indicating an increased level of Tb-O covalency.

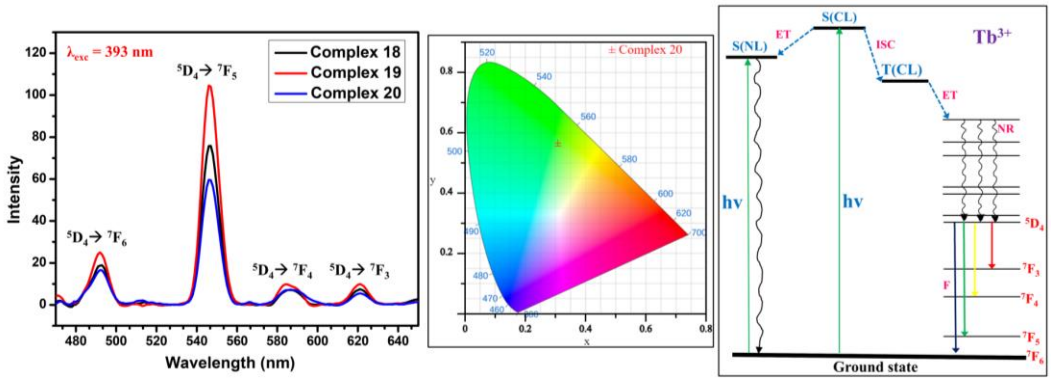

Figure 5.5 The solid-state emission spectra, CIE chromaticity diagram and "Antenna effect" energy diagram for complexes 18-20.

Conclusions

Three Terbium-acylpyrazolone complexes 18, 19, and 20 with eight-coordinated distorted square antiprism geometry were synthesized and characterized. Four transitions, their type, G/B ratio, and chromaticity diagram corresponding to different regions have been examined from the solid-state emission spectra. The transitions $^5D_4 \rightarrow {}^7F_6$ and $^5D_4 \rightarrow {}^7F_5$ are observed in the blue and green regions, respectively, and their G/B ratio is greater than unity (G/B>1), indicating an increased level of Tb-O covalency. The functional group attached to the phenyl rings of acylpyrazolone, an NL (neutral ligand) that provides stability, fluorescence efficacy, absorption efficacy, and LMCT efficacy, has a significant impact on the intensity of solid-state emission spectra as seen in antenna effect energy diagrams.

Chapter 6 Thorium Acylpyrazolone Complexes: Synthesis, Covalent Character, and Crystal Features.

Experimental work

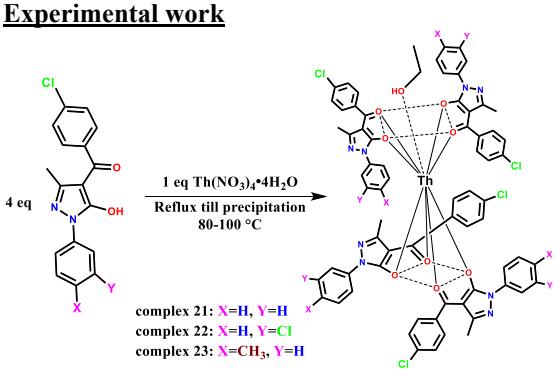

Property	Complex 21	Complex 22	Complex 23
Yield	96.34%	95.94%	94.73%
Melting Point	>200 °C	>200 °C	>200 °C
Mole. Formula	$C_{70}H_{54}Cl_4N_8ThO_9$	$C_{70}H_{50}Cl_8N_8ThO_9$	$C_{74}H_{62}Cl_4N_8ThO_9$
Molecular weight	1539.11	1662.86	1581.20
Λ^s_M (ohm^{-1} cm^{2}mol^{-1})	2.32	2.86	2.50

Figure 6.1 Synthetic route for complexes 21-23.

FTIR spectral analysis

The significant observation is decrease in the $\nu_{C=O\ (benzoyl)}$ and $\nu_{C=O\ (acyl)}$ peak values in complexes compare to similar bands in the ligands (Table 6.1). FTIR spectrum of complex 22 is given in Figure 6.2.

Table 6.1 FTIR spectral analysis of complexes 21-23.

Code	$\nu_{C=O}$ benzoyl	$\nu_{C=O}$ acyl	Cyclic $\nu_{C=N}$	ν_{C-C} aromatic	ν_{N-N}
L_1	1620	1590	1484	1357	1213
Complex 21	1606	1580	1475	1378	1158
L_2	1624	1590	1484	1348	1210
Complex 22	1602	1589	1474	1368	1159
L_3	1694	1601	1446	1381	1178
Complex 23	1648	1597	1474	1382	1163

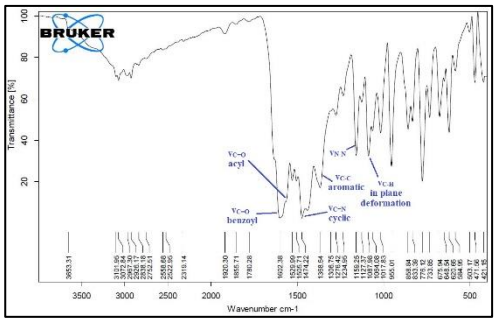

Figure 6.2 FTIR spectrum of complex 22.

Single crystal x-ray diffraction analysis

Figure 6.3 shows the single crystal x-ray structure of complex 22 having triclinic crystal system and *P -1* space group. The lengths of the C-O bonds in the acyl group are slightly higher than typical for C–O distance in ketones (1.23 Å) due to O→Th bonding.

In comparison to Th-O(acyl) bond lengths (2.427–2.476 Å), Th-O(pyrazolone) bond lengths (2.274–2.369 Å) are slightly higher, indicating stronger covalency caused by the acyl group O-atoms. This is because longer bonds lead to a drop in the average bond order between Thorium and O-atoms, increasing covalency.

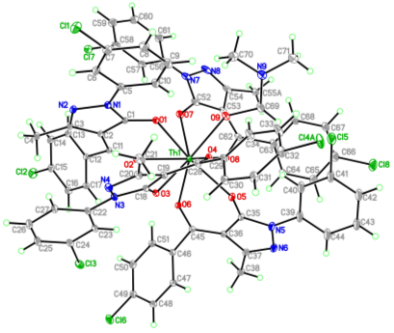

Figure 6.3 ORTEP diagram for complex 22.

Hirshfeld surface area analysis

Using the crystal explorer 17.5 programme, the donor-acceptor interaction sites and intermolecular interactions with neighbouring molecules can be visualised for complex 22 (Figure 6.4).

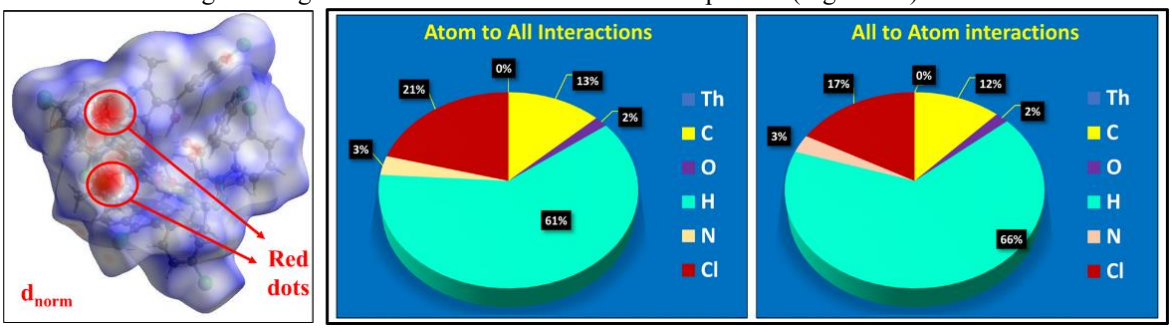

Figure 6.4 Hirshfeld surface and its percentage interactions in complex 22.

Electronic spectral analysis

Electronic spectra of 0.01 M solution of complexes 21, 22, and 23 in various solvents were recorded (Figure 6.5).

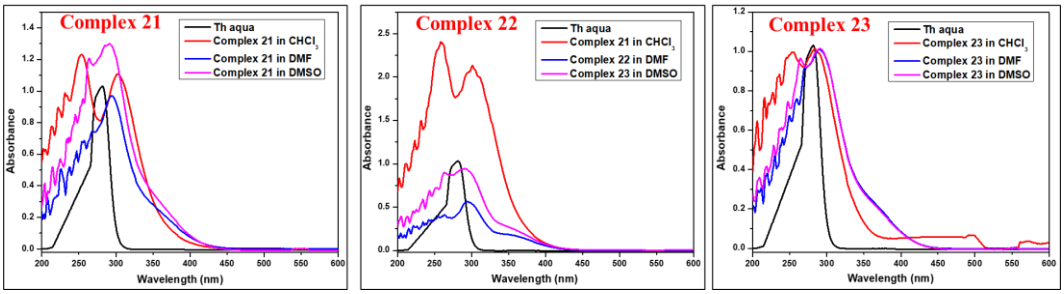

Figure 6.5 Electronic spectra of 0.01 M solution of complexes 21, 22, and 23 in various solvents.

To demonstrate the covalency of complexes 21, 22, and 23, Nephelauxetic ratio (β), Sinha parameter (δ%), bonding parameter ($b^{1/2}$), and angular overlap parameter (η) were calculated using following equations (See Table 6.2). Calculating the covalency parameters demonstrates the electron delocalization across the 4f orbital and the covalency, both positive for all complexes, suggesting an analogous degree of covalent bonding.

$$\text{Nephelauxetic ratio } \boldsymbol{\beta} = \frac{\bar{\nu}_{complex}}{\bar{\nu}_{free\ ion}} \qquad \text{Bonding parameter } b^{\frac{1}{2}} = \left(\frac{1-\beta}{2}\right)^{1/2}$$

$$\text{Sinha parameter } \delta\% = \left[\frac{1-\beta}{\beta}\right] \times 100 \qquad \text{Angular overlap parameter } \eta = \frac{1-\sqrt{\beta}}{\sqrt{\beta}}$$

Table 6.2 Calculation of covalency parameters for complexes 21, 22, and 23.

Complex	Solvent	Peak center (in cm^{-1})	Nephelauxetic ratio B	Bonding parameter $b^{\frac{1}{2}}$	Sinha parameter δ	Angular overlap parameter η
21	$CHCl_3$	39370	0.9511	0.1564	5.141	0.0254
	DMF	34005	0.8215	0.2988	21.7292	0.1033
	DMSO	34341	0.8296	0.2919	20.5381	0.0979
22	$CHCl_3$	39472	0.9536	0.1524	4.8693	0.0241
	DMF	34025	0.822	0.2983	21.6576	0.103
	DMSO	34321	0.8291	0.2923	20.6084	0.0982
23	$CHCl_3$	39356	0.9508	0.1569	5.1784	0.0256
	DMF	34530	0.8342	0.2879	19.8784	0.0949
	DMSO	34344	0.8297	0.2918	20.5276	0.0979

Conclusions

Three monocapped square antiprismatic Thorium complexes were synthesized and characterized using acylpyrazolone ligands. The characterized data are largely used to examine their structure, geometry, composition, surface interactions, and covalent character. Electronic spectral studies were carried out to calculate Covalency parameters (Nephelauxetic ratio, Sinha parameter, Bonding parameter, Angular Overlap Parameter) to get covalency order in different solvents.

Publications from this research

[1] M. Travadi, R.N. Jadeja, R.J. Butcher, J Mol Struct. 1318 (2024) 139295.
[2] M. Travadi, R. N. Jadeja, R. J. Butcher, Polyhedron. 247 (2024) 116701.
[3] M. Travadi, R. N. Jadeja, R. J. Butcher, M.S. Shekhawat, Inorganica Chim Acta. 559 (2024) 121766.
[4] M. Travadi, R. N. Jadeja, R. J. Butcher, ChemistrySelect. 8 (2023) e202302438.
[5] M. Travadi, R. N. Jadeja, R. J. Butcher, J Mol Struct. 1281 (2023) 135137.
[6] M. Travadi, R. N. Jadeja, R. J. Butcher, ACS Omega. 7 (2022) 34359–34369.
[7] M. Travadi, R. N. Jadeja, R. J. Butcher, Polyhedron. 223 (2022) 115956.
[8] M. Travadi, R.N. Jadeja, R.J. Butcher, (Manuscript accepted in ChemistrySelect journal on 17th October, 2024)

References

[1] B. Keshavan, P. G. Chandrashekara, N. M. M. Gowda, J Mol Struct. 553 (2000) 193–197.

[2] S. SeethaLekshmi, A.R. Ramya, M. L. P. Reddy, S. Varughese, Journal of Photochemistry and Photobiology C: Photochemistry Reviews. 33 (2017) 109–131.

[3] U. N. Tripathi, P. P. Bipin, R. Mirza, S. Shukla, J Coord Chem. 55 (2002) 1111–1118.

[4] S. Singh, P. Bhardwaj, J. Alloys Compd. 509 (2011) 7047–7051.

[5] P. Ahlawat, S. Bhayana, V. Lather, S. Khatri, P. Kumari, M. Kumar, M. S. Shekhawat, V. B. Taxak, S. P. Khatkar, R. Kumar, Opt Mater (Amst). 133 (2022) 112940.

[6] I. Ameen, A. K. Tripathi, R. L. Mishra, A. Siddiqui, U. N. Tripathi, Karbala International Journal of Modern Science. 4 (2018) 258–273.

[7] M. A. Gagnani, R. S. Shukla, S. N. Misra, Spectrochim Acta A Mol Biomol Spectrosc. 61 (2005) 535–539.

[8] D. Prasad, A. Praveen, S. Mahapatra, S. Mogurampelly, S. R. Chaudhari, Food Chem. 361 (2021) 130000.

[9] T. Qin, Z. Shi, W. Zhang, X. Dong, N. An, H. Sakiyama, M. Muddassir, D. Srivastava, A. Kumar, J Mol Struct. 1282 (2023) 135220.

[10] F. Marchetti, R. Pettinari, C. Pettinari, Coord Chem Rev. 303 (2015) 1–31.

[11] M. A. Neelakantan, V. Latha, S. Thalamuthu, J Mol Struct. 1249 (2022) 131573.

[12] S. Muhammad, S. Kumar, J. Koh, M. Saravanabhavan, K. Ayub, M. Chaudhary, Mol Simul. 44 (2018) 1191–1199.

[13] Jensen, B. Skytte, Acta Chemica Scandinavica, Acta Chem Scand. 13 (1959) 1668–1670.

[14] R. N. Patel, Y. Singh, Y. P. Singh, A. K. Patel, N. Patel, R. Singh, R. J. Butcher, J. P. Jasinski, E. Colacio, M. A. Palacios, New J Chem. 42 (2018) 3112–3136.

[15] W. T. Carnall, P. R. Fields, B. G. Wybourne, J Chem Phys. 42 (1965) 3797–3806.